

This article was downloaded by:

On: 21 January 2011

Access details: *Access Details: Free Access*

Publisher *Taylor & Francis*

Informa Ltd Registered in England and Wales Registered Number: 1072954 Registered office: Mortimer House, 37-41 Mortimer Street, London W1T 3JH, UK



The Journal of Adhesion

Publication details, including instructions for authors and subscription information:

<http://www.informaworld.com/smpp/title~content=t713453635>

Adhesion of Patterned Reactive Interfaces

Edwin P. Chan^a; Dongchan Ahn^b; Alfred J. Crosby^a

^a Department of Polymer Science and Engineering, University of Massachusetts, Amherst, Massachusetts, USA ^b Dow Corning Corporation, Midland, Michigan, USA

To cite this Article Chan, Edwin P. , Ahn, Dongchan and Crosby, Alfred J.(2007) 'Adhesion of Patterned Reactive Interfaces', The Journal of Adhesion, 83: 5, 473 – 489

To link to this Article: DOI: 10.1080/00218460701377628

URL: <http://dx.doi.org/10.1080/00218460701377628>

PLEASE SCROLL DOWN FOR ARTICLE

Full terms and conditions of use: <http://www.informaworld.com/terms-and-conditions-of-access.pdf>

This article may be used for research, teaching and private study purposes. Any substantial or systematic reproduction, re-distribution, re-selling, loan or sub-licensing, systematic supply or distribution in any form to anyone is expressly forbidden.

The publisher does not give any warranty express or implied or make any representation that the contents will be complete or accurate or up to date. The accuracy of any instructions, formulae and drug doses should be independently verified with primary sources. The publisher shall not be liable for any loss, actions, claims, proceedings, demand or costs or damages whatsoever or howsoever caused arising directly or indirectly in connection with or arising out of the use of this material.

Adhesion of Patterned Reactive Interfaces

Edwin P. Chan,

Department of Polymer Science and Engineering, University of
Massachusetts, Amherst, Massachusetts, USA

Dongchan Ahn

Dow Corning Corporation, Midland, Michigan, USA

Alfred J. Crosby

Department of Polymer Science and Engineering, University of
Massachusetts, Amherst, Massachusetts, USA

We demonstrate the role of chemical surface patterns on the adhesion of soft, elastomeric interfaces. The microscale patterns consist of periodic variation of two types of silane surface chemistries: a reactive silane that bonds covalently with the soft elastomer and a passive silane that is weakly adhered with the elastomer. Using an adhesion test based on 90° peel geometry, we demonstrate that the tuning of adhesion depends on the spatial distribution of the reactive silane groups. Given our material system and pattern symmetries, an enhancement in adhesion energy is observed in a majority of the patterns. The mechanism of enhancement is associated with the shape of the contact line. Specifically, the reactive silane interfaces play a significant role in defining the width of the contact line. In instances where enhancement is observed, the width of the contact line increases because of the “pinning” of the contact line by the reactive interfaces. These results emphasize the importance of contact line interaction with the pattern shapes and demonstrate opportunities for using well-defined two-dimensional patterns to actively tune polymer adhesion.

Keywords: Adhesion; Elastomer; Peel test; Reactive interfaces; Silane; Surface chemical patterns

Received 16 December 2006; in final form 26 March 2007.

One of a Collection of papers honoring Liliane Léger, the recipient in February 2007 of the *Adhesion Society Award for Excellence in Adhesion Science, Sponsored by 3M*.

Address correspondence to Alfred J. Crosby, Department of Polymer Science and Engineering, University of Massachusetts, Amherst, MA 01003-9263, USA. E-mail: crosby@mail.pse.umass.edu

INTRODUCTION

Nature has demonstrated that a powerful design strategy for tuning adhesion lies in the development of microscale-patterned structures at an interface [1,2]. Inspired by these natural attachment systems (*i.e.*, gecko and jumping spider), researchers have adopted similar strategies in controlling polymer adhesion [3–10]. In a majority of these systems, the structured polymer interfaces are topographically patterned with micro- and nanoscale surface post-like structures. Several research groups have demonstrated that the post-like structures tune adhesion by controlling the stability of the interfacial separation event, which is defined by the lateral dimensions of the post a [8,9]. Adhesion is optimized when a approaches a critical length scale a^* , which defines the change in the local mode of separation from initiation driven to propagation dominated. This length scale a^* is a material-defined parameter that is related to the ratio of critical energy-release rate \mathcal{G}_c and elastic modulus E .

The materials-defined length scale, a^* , gives insight into a practical guideline in pattern design because it suggests that the optimal pattern dimension is defined by the ratio of \mathcal{G}_c/E . Because this design criterion is defined solely by the local materials' properties, the types of structured surfaces are not limited to surface relief-type interfaces. For example, we can consider a surface chemical pattern, which is a patterned surface defined by a periodic variation in surface chemical properties.

Surface chemical patterns provide several benefits in controlling adhesion compared with topographic patterns. First, unlike post structures, issues associated with pattern collapse are avoided. In the example of the synthetic "gecko tape," the adhesive properties of the interface degrade as a result of "condensation" of the fibrillar structures [4]. Over the course of multiple attachment–detachment cycles, the condensation process will result in a decrease in adhesive strength. Second, because the patterns are chemical in nature, virtually no surface topology exists. Creating controlled surface topology requires molding or vertical deposition, which is typically more process intensive than two-dimensional patterning. In instances where large variations in surface topography are undesirable or impractical to implement but adhesion control is still necessary, such as for tissue engineering, surface patterns are ideal patterned interfaces for cell culture [11,12]. Third, surface chemical patterns can be optically transparent. With surface relief patterns, because of the scattering contrast of the microscale post structures, the textured surface will be opaque. In applications where visual clarity is desired (*i.e.*,

windshields), surface-chemical patterns facilitate this requirement while still providing adhesion control.

Although natural attachment devices such as the gecko and jumping spider rely remarkably well on topographic patterns that provide the benefits of reversibility (noncovalent interactions) and self-cleaning properties, these interactions cannot withstand the nonbiological or environmental conditions found in many industrial applications, such as under the hood of an automobile, where resistance to extreme temperature variations, harsh solvents, and mechanical stresses is critical to reliability. Hence, wet-dispensed adhesives (as opposed to pressure-sensitive adhesives, PSAs) rely on irreversible chemical bonds for structural bonding and sealing. Because adhesives are typically applied as a macroscopic continuum relative to the length-scale represented by a^* , the effect of pattern density is not well established. The effect of coupling biologically inspired pattern control principles with irreversible, industrial-strength synthetic interactions are unknown.

In this article, we explore the influence of surface chemical patterns on the adhesion of soft, elastomeric interfaces. Specifically, the microscale patterns consist of periodic variations of two silanes—a reactive silane that covalently bonds to the elastomer and an inert silane that is weakly adhered with the elastomer. To explore the interaction of chemical patterns with the soft elastomer, we focus on three types of pattern geometry with pattern dimensions on the microscale (circles, triangles, and lines). We demonstrate that the reactive silane regions determine the adhesive properties of the patterned interfaces. More important, the mechanisms of adhesion are determined by the spatial distribution of the reactive silanes. In the following sections, we describe our experimental approach, an overview of the results and a discussion of the mechanisms of adhesion for the surface chemical patterned interfaces.

EXPERIMENTAL APPROACH

Pattern Fabrication

We prepare surface chemical patterns on glass substrates using a combination of conventional UV photolithography and selective silane chemistry [13,14]. Selective regions of the substrate are coated with 3-aminopropyl triethoxy silane (r-SAM). The amine is the reactive species that can form covalent bonds with the epoxide groups available in the epoxy-functionalized polydimethyl siloxane elastomer (e-PDMS). The remainder of the glass surface is coated with *n*-octyl trichloro silane (i-SAM), which is chemically inert with the elastomer. To explore the effects of pattern dimensions, we used a combinatorial approach

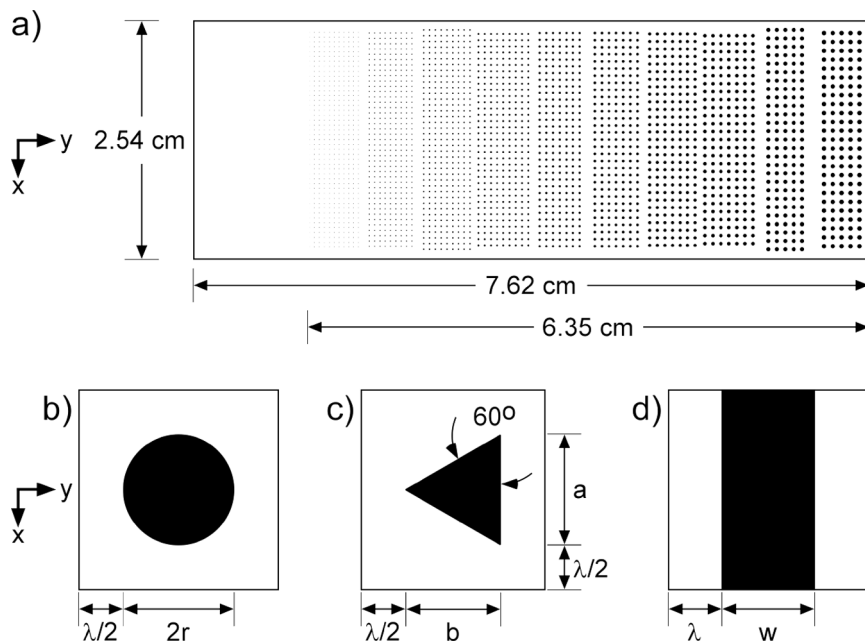
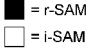
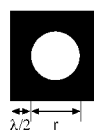
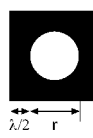
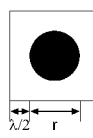
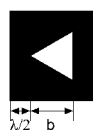
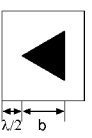
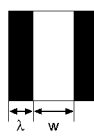
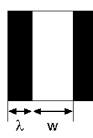



FIGURE 1 a) Overall dimensions of a combinatorial library of patterns for a single peel sample. A single peel sample (with overall dimensions of 7.6 cm by 2.5 cm) consists of 10 separate pattern densities (different pattern size but same spacing). The three different types of pattern shapes include b) circles, c) triangles, and d) lines. The y -direction represents the peel direction. The dimensions of the 3 patterns correspond to the values listed in Table 1.

where a single glass substrate consists of a library of 10 patterns of different dimensions (Figure 1a). In addition, to explore the effects of pattern shapes, we prepared three types of patterned surfaces that included libraries of circles, triangles, and lines (Figure 1c, d). The dimensions for all the patterns explored in this work are summarized in Table 1.

The surface chemical patterns were prepared by sequential vapor-phase deposition of two silane self-assembled monolayers (Gelest Inc., Morrisville, PA, USA) onto a glass substrate prepared by conventional photolithography. The patterning procedure is summarized in Figure 2. We began by coating i-SAM onto a 7.6-cm by 2.5-cm glass substrate by vapor-phase deposition (Figure 2a–g). Next, a photoresist layer (Rohm & Hass SPR220, supplied by Microchem Corp., Newton, MA, USA) was spun-coated over the entire i-SAM monolayer surface. The photoresist was patterned by UV exposure (OAI, $\lambda = 365$ nm, OAI, San Jose, CA, USA) through a photomask (Pageworks, Cambridge,

TABLE 1 Summary of Pattern Shapes and Dimensions Explored

Sample Name	C ₁	C ₂	C ₃	T ₁	T ₂	L ₁	L ₂
Pattern geometry 							
Dimensions	250	λ (μm) 500	500	250	λ (μm) 500	250	λ (μm) 500
increasing r-SAM density 	250 225 200 175 150 125 100 75 50 25	r (μm) 250 225 200 175 150 125 100 75 50 25	25 50 75 100 125 150 175 200 225 250	b (μm) 1370 1116 907 732 582 452 338 239 150 71	69 142 219 300 386 477 574 677 786 903	w (μm) 268 240 212 182 153 122 92 62 34 11	244 214 184 154 124 96 69 44 22 7

MA, USA) and then developed, which exposed the underlying i-SAM layer. Subsequent UV/ozone oxidation chemically cleaved the exposed i-SAM regions [13]. Thorough rinsing with toluene removed the cleaved silanes as well as the photoresist layer. Next, r-SAM was patterned over the exposed glass substrate surface (Figure 2h–i). Through vapor-phase deposition, the r-SAM reacted with the exposed, bare glass surface and completed the surface chemical patterning process to generate periodic regions of i-SAM and r-SAM. Finally, the surface was rinsed thoroughly with toluene to remove unreacted r-SAM silanes. The fidelity of the patterns was qualitatively evaluated by condensation of water onto the surface chemical patterned surfaces, and the patterned surfaces were used without further treatment.

Materials

We used films of e-PDMS elastomer as the model adhesive in our peel experiments. The e-PDMS (Dow Corning Corp., Midland, MI, USA) was prepared by mixing 65% (w/w) dimethylvinylsiloxy-terminated PDMS, 25% vinyl functional (2 wt%) silicate resin, 0.2% Karstedt's platinum catalyst complex dispersed in PDMS, and 10% telechelic PDMS oligomer multifunctional in silicon hydride groups that was pre-functionalized by partial substitution of the silicon hydride with epoxy groups. Because the elastomer used is a custom material, we measured the viscoelastic response of the elastomer. Based on dynamic mechanical testing, we measured the $E' \sim \omega^{0.04}$ and $E'' \sim \omega^{0.14}$ over the frequency (ω)

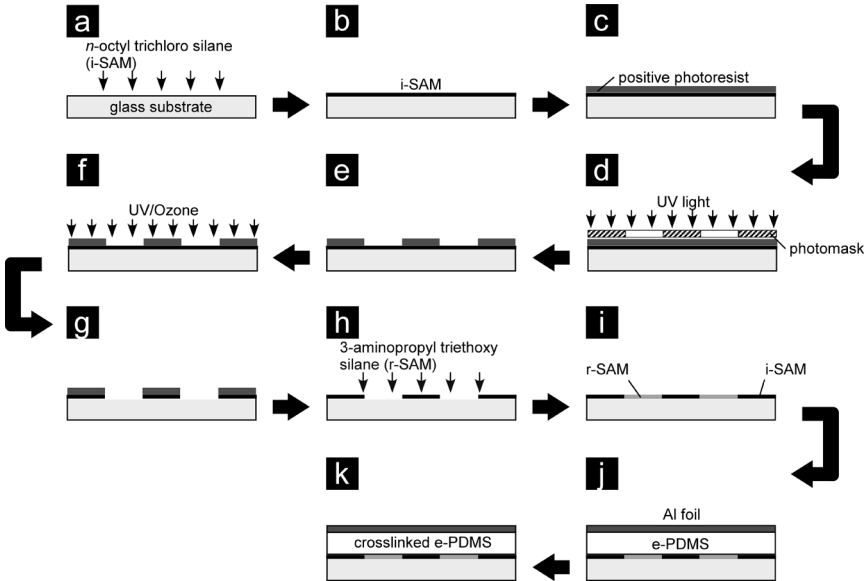


FIGURE 2 Procedure for fabricating the surface chemical patterns: a) and b) The entire glass substrate is coated with *n*-octyl trichloro silane (i-SAM) by vapor-phase deposition. c) The i-SAM surface is then covered by a spun-cast photoresist layer. d) and e) Upon UV exposure through a photomask and subsequent development, selective regions of the i-SAM surface becomes exposed. f) UV/ozone treatment of the exposed i-SAM chemically cleaves the silane from the glass surface. g) Rinsing with toluene removes the cleaved i-SAM and the remaining resist layer. h) The bare glass regions are coated with 3-aminopropyl triethoxy silane (r-SAM) by vapor-phase deposition. i) This yields the surface chemical patterns of alternating i-SAM and r-SAM regions. j) and k) Reaction and cross-linking of the epoxy-modified polydimethyl siloxane (e-PDMS). The e-PDMS mixture is poured over the patterns and then heat cured at 150°C for 30 min. Copper wire spacers are used to maintain the thickness of the elastomer. An aluminum foil backing is used to increase the stiffness of the elastomer.

range of 0.01 to 10 Hz. To obtain the elastomer films for peel tests, the e-PDMS mixture was deposited onto the patterned surface and then doctored with a leveling blade to ensure uniform film thickness (thickness = 0.90 mm). A superstrate backing layer consisting of aluminum foil (thickness = 0.15 mm) was placed on top of the e-PDMS layer, while spacer blocks of copper wire were used to maintain the e-PDMS film thickness. The samples were then heated at 150°C for 30 min, which cured the e-PDMS while at the same time allowed for the chemical bonding of the epoxy groups of the e-PDMS with the r-SAM layer.

Adhesion Experiments

We measured the adhesion of the patterned interfaces using 90° peel tests. Prior to the test, the sides of elastomer were trimmed to obtain a center peel strip with a width of 2.2 cm. This trimming was intended to eliminate edge effects that arise because of the changes in stiffness as a result in changes in the film thickness near the edges of the film. The peel tests were conducted with an Instron tensile mechanical tester (MTS Sintech 5/G, MTS Systems Corporation, Eden Prairie, Minnesota, USA). To begin the peel test, the glass substrate was secured onto a frictionless moving stage (MTS 90-Degree Peel Fixture). A short section of the aluminum-backed elastomer was bent backward 90° and allowed for the attachment to the upper grip of the mechanical tester. The peel angle was maintained throughout the test by a pulley system that ensured the moving stage moves in unison with the upper grip. The specimen is then separated by retracting the upper grip at a constant crosshead velocity of $42 \mu\text{m/s}$. The data collection rate was approximately 1 data point/s, which was sufficient to observe the pattern interaction with the elastomer.

Representative load (P)–displacement (δ) curves for an unpatterned and patterned peel tests experiment are illustrated in Figure 3. Following the initial sudden increase in peel force due to the initiation

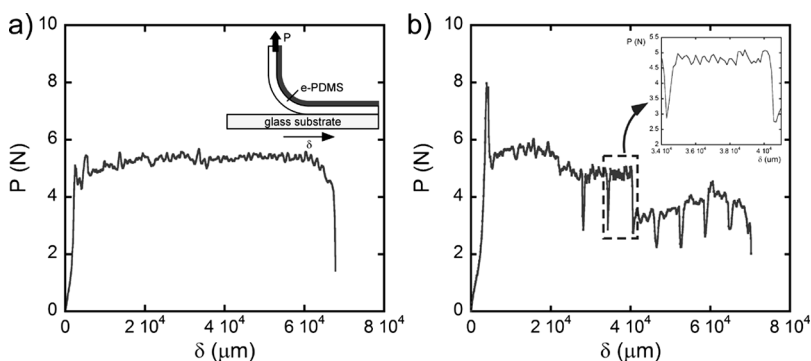


FIGURE 3 a) The force (P) vs. displacement (δ) result for a peel test of a homogeneous surface of 3-amino triethoxypropyl silane monolayer (r-SAM). The average peel force P_m is quantified by averaging the steady-state values over the entire crack propagation period. b) The force vs. displacement for a representative combinatorial library of patterned surface consisting of 10 patterns. The inset highlights the response for a single pattern density. The unpatterned region that separates the patterned surfaces is identified by the sharp decrease in force.

of a crack, the peel force reached a steady-state value that is associated with the propagation of the crack. We quantified an average peel force (P_m) by averaging the steady-state values over the entire crack-propagation period. For the unpatterned peel data, the entire surface consisted of a homogenous coverage of r-SAM layer; therefore, the steady-state peel force remained constant. Postinspection of the glass substrate revealed that a thin layer of the elastomer remained on the surface, suggesting that the separation process occurred through the cohesive fracture of the elastomer near the silane–elastomer interface. Similarly, for the patterned surface, we observed cohesive fracture of the elastomer in the r-SAM regions, and the i-SAM regions failed adhesively. From these results, along with knowledge of the geometry of the elastomer, we quantified a lower limit of the critical energy-release rate (\mathcal{G}_c) of the interface. In the peel test geometry, \mathcal{G}_c is related to the peel force, the adhesive width (w), and the peel angle (θ) by the Kaelble equation [10]:

$$\mathcal{G}_c = \frac{P}{w} \cdot (1 - \cos\theta). \quad (1)$$

For our peel geometry ($\theta = 90^\circ$), \mathcal{G}_c reduced to P/w . As \mathcal{G}_c is a materials-defined parameter and therefore independent of interfacial contact, the descriptor was especially insightful in quantifying adhesion for all the surface chemical patterns explored in this work. For the homogeneous i-SAM surface, we were unable to quantify the peel force because we consistently obtained an average force value that was less than the resolution of the instrument. Therefore, the upper bound for \mathcal{G}_c for the i-SAM interface is defined as the resolution of our instrument: 4.5 J/m^2 . For the r-SAM interface, we measured \mathcal{G}_c equal to 242.0 J/m^2 . This quantity is a lower bound because cohesive failure in the e-PDMS is observed visually. These values define material length scales, \mathcal{G}_c/E , that are approximately $200 \mu\text{m}$ for the r-SAM interface and $5.0 \mu\text{m}$ for the i-SAM. Accordingly, our pattern dimensions (Table 1) were designed to be commensurate with these material length scales. Furthermore, our film is sufficiently thick such that the dissipation process is confined to the interface of the elastomer and chemical pattern surface.

We also used the 90° degree peel test to quantify adhesion for the combinatorial library of surface chemical patterns. For each pattern within the combinatorial library, we defined a discrete value of P_m by averaging the steady-state peel force over the length of the specific pattern. In addition to P_m , we used the materials-defined adhesion descriptor \mathcal{G}_c to elucidate the effects of surface density of the r-SAM species.

RESULTS

The adhesion of binary–silane interfaces has been studied previously by several research groups. However, the previously explored binary–silane interfaces are unpatterned surfaces that consist of random distribution of silane groups [15,16]. Hence, the role of periodic surface chemistry on adhesion remained unexplored. In this work, the surface chemical patterns represent model systems to study the impact of periodic variation in interfacial bond strength on the overall adhesive properties. To compare the pattern surfaces, we evaluated the patterns independent of the pattern shapes and dimensions by quantifying the surface density of chemically bonded r-SAM species. In relating P_m to r-SAM surface density, the line fraction is the appropriate parameter because the peel force is directly proportional to the width of the adhesive. If we consider the y -axis as the peel direction (Figure 4), the average line fraction of the r-SAM region f_r is defined by the lateral dimensions of the r-SAM region normalized by the entire width of the unit cell (W).

$$f_r = \frac{\int_0^L [w(y) \cdot dy/W]}{\int_0^L dy} \quad (2)$$

The integration limit, L , is defined by the y -axis limit of the unit cell. The average line fraction (f_r) as defined by Eq. (2) is equivalent to the area fraction (ϕ_r) of the pattern. The average peel force results for the peel tests are presented in Figure 5. Given our material system and the patterns explored, we were able to tune P_m from 20% to 115%

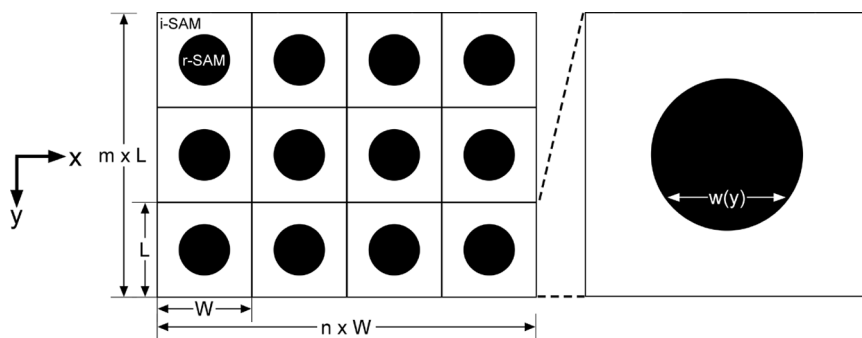


FIGURE 4 Example of a pattern surface consisting of circular patches of r-SAM in a matrix of i-SAM. The pattern consists of n rows and m columns of unit cells of dimensions $W \times L$. If we consider the peel direction along the y -axis, the line fraction is defined as $w(y)/W$.

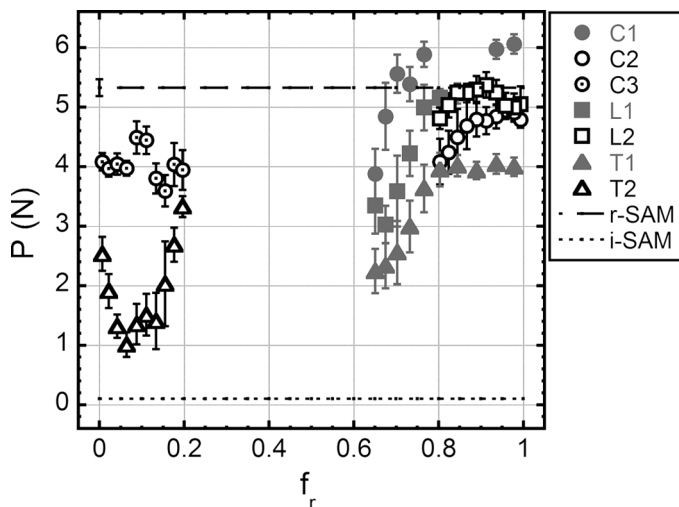


FIGURE 5 Plot summarizing the peel test results for all the materials explored. Each sample represents a combinatorial library consisting of 10 test patterns with the same pattern shape but different pattern dimensions as evidenced by the variation in average line fraction (f_r). a) P_m as a function of (f_r) for all the surface chemical patterns explored in this work. To identify the effects of surface coverage on adhesion, we evaluate the patterns in terms of an average line fraction of r-SAM. As a comparison, P_m for the nonpatterned reactive (r-SAM) and inert (i-SAM) silane surfaces are also presented. As we are unable to quantify P_m for the i-SAM surface, we estimate the value as the lower resolution of the peel test instrument, which is ~ 0.1 N.

compared with P_m for the unpatterned r-SAM surface. Figure 5 illustrates this effect as a function of f_r . While these results demonstrate the tuning of adhesion with well-defined patterns of surface chemistry, they also suggest that all three classes of patterns respond differently—*i.e.*, mechanisms beyond the straightforward contribution of surface density of the reactive silane.

To identify a universal behavior, we use \mathcal{G}_c to quantify the adhesion for all the pattern surfaces as a function of area fraction of the reactive regions. Figure 6 summarizes these results in terms of normalized \mathcal{G}_c ($\overline{\mathcal{G}}_c$), where the values of energy-release rate are normalized by the value for the unpatterned r-SAM interface. The results demonstrate that the response is not universal among all the patterns and suggest that the adhesion cannot be described simply by the surface density of the reactive silane interfaces. As we discuss in the following section, pattern geometry plays a significant role in controlling adhesion and can be used as an effective parameter in interfacial design.

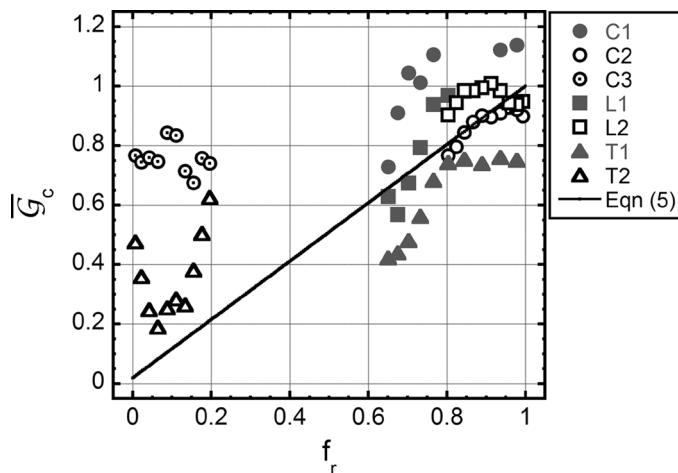


FIGURE 6 Plot of adhesion energy (G_c) versus line fraction (f_r). The adhesion energy is normalized by the adhesion energy of the r-SAM (G_r). The solid curve represents the prediction of Eq. (5) where we assume G_c scales with the area fraction of the r-SAM and i-SAM.

DISCUSSION

If regions in a patterned interface obey a simple rule of mixtures, the total peel force (P_{avg}) can be simply defined as the sum of the individual contributions from the r-SAM (P_r) and i-SAM (P_i) regions:

$$P_{avg} = P_r + P_i. \quad (3)$$

Based on Eq. (1), we can use the measured energy-release rates for the r-SAM (G_r) and i-SAM (G_i) surfaces and the known average line widths for these respective regions (w_r and w_i) to yield the following expression for the effective G_c for the patterned interface:

$$G_c = \frac{P_{avg}}{w} = \frac{w_r G_r + w_i G_i}{w}. \quad (4)$$

Defining w_r/w as the average line fraction [Eq. (2)] and normalizing by G_r , we obtain the normalized energy-release rate for a binary surface chemical pattern.

$$\bar{G}_c = \frac{G_i}{G_r} + \left(1 - \frac{G_i}{G_r}\right) \cdot f_r. \quad (5)$$

Equation (5) predicts that an increase in the average line fraction of the reactive silane will simply lead to a proportional enhancement in the adhesion energy. In essence, this equation is insensitive to pattern

geometry because it considers the surface as an unspecified distribution of r-SAM and i-SAM silane groups with the response from neighboring regions being uncoupled. Therefore, any deviation of adhesion energy from the prediction by Eq. (5) implies that the pattern geometry plays an important role in tuning adhesion.

Based on the results shown in Figure 6, almost all the patterns demonstrate an enhancement in adhesion compared with the rule of mixture prediction. More important, the adhesion is maximized well below maximum f_r ($= 1$). With the circular patterns of C1, \bar{G}_c reaches unity at $f_r \sim 0.7$. In fact, the maximum adhesion energy for this pattern library is approximately 115% greater compared with a smooth, unpatterned reactive interface. Other patterns demonstrate similar optimization of adhesion energy well below maximum line fraction; however, the circular patterns provide the greatest enhancement. As we discuss in the following section, the mechanism of enhancement for all the patterns is attributed to pattern geometry (which includes feature shape, feature arrangement, and feature spacing) increasing the width of the contact line, which serves to enhance the interfacial resistance to crack propagation.

Contact Line Resistance

With the exception of the triangular pattern library of T1, all pattern libraries demonstrate an enhancement in adhesion energy relative to the prediction of Eq. (5). This enhancement is related to the lengthening of the contact line as a result of contact line pinning. With a homogeneous unpatterned interface, the contact line is equivalent to the width of the adhesive. By incorporating periodic regions of surface chemical contrast, the contact line profile will increase as a function of the surface chemistry contrast and the perimeter of the pattern region. To understand this mechanism for the pattern libraries of C3 and T2, we consider these surfaces as homogeneous i-SAM surfaces with the r-SAM species occupying discrete regions of the interface. As illustrated in Figure 7, the separation process can be described as the opening of a crack, where the contact line defines the crack front during the peel experiment. Prior to interacting with the discrete patterns, the width of the contact line corresponds to the width of the adhesive (Figure 7a-i, 7b-i). Once the crack front approaches discrete r-SAM patterns, the presence of the r-SAM regions “pins” the contact line (Figure 7a-ii, 7b-ii). This leads to the deformed, lengthened profile of the contact line, which increases the resistance for the crack to propagate. As a result, additional energy must be supplied to drive the crack forward. The enhancement is more significant for

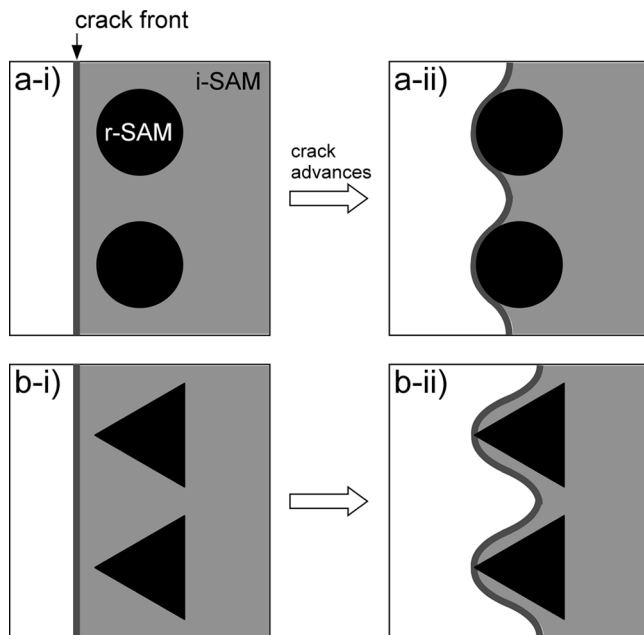


FIGURE 7 Illustration of the contact line resistance for the discrete r-SAM patterns of C3 and T2. As the crack front advances, the contact line becomes “pinned” by the discrete r-SAM triangular regions. As a result, additional energy must be supplied to drive the crack forward, which leads to an increase in adhesion energy for the interfaces. The grey-shaded area is the interface that remains in intimate contact.

C3 compared with T2, which we believe is associated with the stress-concentrating geometry presented by the aligned triangles. In other words, the circular geometry blunts the contact line more effectively than the triangular patterns. Hence, an r-SAM circular geometry (with the same area as the triangle) will provide greater efficiency in pinning the contact line than the r-SAM triangular geometry. This mechanism is analogous to the Cook–Gordon mechanism of crack blunting in laminate composite materials [17]. A similar mechanism of adhesion enhancement has been previously observed by Chung and Chaudhury for topographically patterned adhesives [18]. Because the crack is forced to deflect laterally, additional energy must be applied to “re-initiate” the separation process. Because this mechanism exists for all the patterns, we observe an enhancement in adhesion for our materials. Although our results show a modest enhancement, based on the results by Chung and Chaudhury

[18], we expect significant enhancement with an optimized patterned interface.

A similar mechanism of contact line pinning is demonstrated for the remaining patterns of C1, C2, L1, L2, and T1. For these systems, the homogeneous phase of the interface is the reactive r-SAM patterned with discrete nonreactive i-SAM. Once again, the presence of the r-SAM matrix effectively “pins” the contact line, which leads to an enhancement of adhesion (Figure 8). The exception is the triangular pattern T1. The adhesion energies for all the patterns within this library are less than the values predicted by Eq. (5). We explain this decrease in the T1 patterns by comparing the crack propagation process between the circular (C1 or C2) and triangular patterns (T1) (Figure 8). Prior to approaching i-SAM patterns as defined by point A, the crack fronts for both patterns are identical (Figure 8a-ii, 8b-ii). Upon interacting with the i-SAM patterns, the contact line widens because of the previously described “pinning” effect. Similar to the r-SAM patterns, this mechanism of adhesion should persist through the entire i-SAM patterns. However, unique to the i-SAM patterns is the control of the contact-line stability as the crack front interacts with the pattern region (from point A to B).

Specifically, the r-SAM region between adjacent i-SAM patterns defines the contact line stability. For the triangular pattern, as the crack front travels from A to B, the interfacial width of the r-SAM region (*i.e.*, the stronger interface) continues to decrease. Hence, an excess of elastic energy is available for the propagation of the crack. From a fracture mechanics standpoint, this crack-separation process is defined as an unstable propagation because $\partial G/\partial \delta \leq 0$. Similarly, the i-SAM circular pattern gives rise to the same mechanism of unstable crack propagation between the points A and A'. However, as the crack travels from A' to B, the interfacial area of the r-SAM region increases for the circular patterns; therefore, additional energy must be supplied to maintain the propagation of the crack. This region is defined as a stable crack-propagation region because $\partial G/\partial \delta \geq 0$. Therefore, the primary distinction between the two patterns in tuning adhesion is attributed to the symmetry of the shapes. Because of the orientation and symmetry of the triangular pattern with the crack-propagation direction, the crack propagation will always be unstable, whereas with the circular patterns, the sequence of unstable–stable crack propagation will persist locally with every circular pattern. However, regardless of the pattern symmetry, our results illustrate the importance of defining the contact line in tuning adhesion, which has been shown by several research groups to be an important parameter in controlling interfacial separation [9,19]. The distinction with

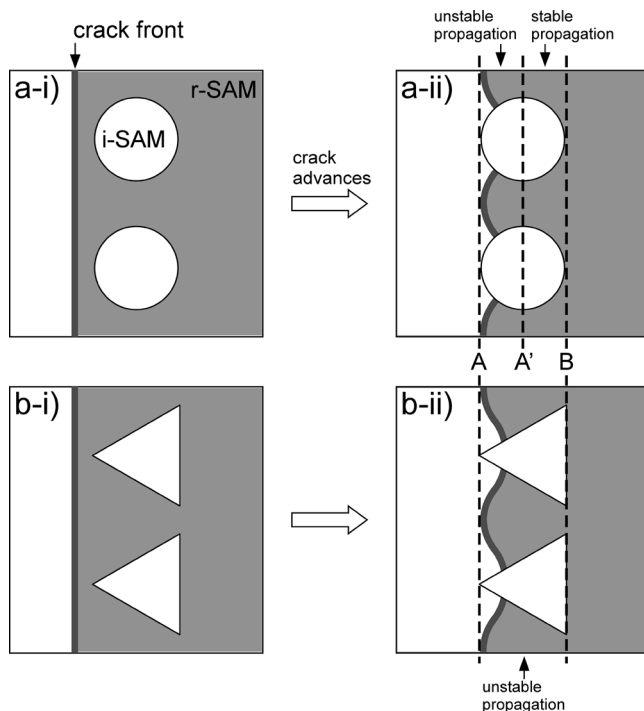


FIGURE 8 Illustration of contact line resistance for the discrete i-SAM patterns. Again, prior to interaction with the i-SAM pattern, the contact line is linear. However, upon interaction with the pattern, the contact line becomes sinusoidal as it is pinned by the r-SAM matrix regions. a-ii) For the circles of i-SAM, the crack propagates initially in an unstable manner from path A to A' because the interfacial contact of the r-SAM regions is continually decreasing. However, from path A' to B, the interfacial contact of the r-SAM gradually increases, which leads the crack to propagate in a stable manner. b-ii) For the triangular pattern, the interfacial contact continues to decrease for the entire path from A to B. Therefore, the crack self-propagates in an unstable manner within this entire region.

our materials systems is that we demonstrate similar mechanisms of enhancement with surface chemical patterns as opposed to surface relief patterns. Finally, the plateau in \mathcal{G}_c for high f_r is attributed to the loss of efficiency of the pattern to lengthen the contact line. For our patterns, because we maintain the same feature spacing, the number density of the features decreases as the feature size increases (*i.e.*, as f_r increases). Hence, the contact line does not increase significantly at high f_r .

SUMMARY

In this work, we have demonstrated the impact of patterned reactive sites on controlling adhesion and have provided simple examples of how the distribution of reactive groups can greatly influence the development of interfacial strength. The lessons learned offer many exciting avenues to develop design guidelines for optimizing interfacial strength. Specifically, we demonstrate the role of surface chemical patterns in tuning the adhesion of soft elastomers. The results of the adhesion tests illustrate the importance of pattern length scale—*i.e.*, pattern dimensions commensurate with material-defined length scale of G_c/E play an important role in tuning adhesion. In all of our material systems and patterned surfaces, the changes in adhesion with f_r cannot be simply described as a random mixture of reactive–nonreactive silanes. Rather, the control of adhesion is connected with the spatial distribution of the reactive silane regions. We observe an enhancement in adhesion in almost all the pattern surfaces. The mechanism of enhancement is associated with the increase in the contact line during separation. Because of the presence of the reactive surfaces, the contact line becomes “pinned” in the r-SAM regions. As a result, additional energy must be supplied to continue propagating the crack. Another mechanism of adhesion that is present in the discrete i-SAM patterns involves the local control of crack-propagation stability. Because of the continual decrease in the r-SAM interfacial area between adjacent i-SAM triangles, the crack propagates in an unstable manner as there is sufficient elastic energy to cause the crack to self-propagate. Hence, this leads to a decrease in the adhesion energy for the all the i-SAM triangular patterns. With the circular, or symmetric, patterns, we observe two stages of crack propagation; the crack initially propagates in an unstable manner and then by stable crack propagation. We expect that the sequence of unstable to stable crack propagation observed in the circular pattern can be reproduced in the triangular pattern by generating a mirrored image of the pattern—*i.e.*, diamond patterns. Although the e-PDMS material used for this study is essentially frequency independent at room temperature, the impact of viscoelastic contributions on the effect of patterned reactive interfaces is an interesting focus for future research.

ACKNOWLEDGMENTS

The authors acknowledge K. A. Weir for helpful suggestions for surface chemical patterning and P. C. Van Dort for providing the

e-PDMS. Funding for this work has been provided by Dow Corning Corporation and NSF CAREER Award DMR-0349078.

REFERENCES

- [1] Arzt, E., Gorb, S., and Spolenak, R., *Proc. Natl. Acad. Sci. U.S.A.* **100**, 10603–10606 (2003).
- [2] Autumn, K., Liang, Y. A., Hsieh, S. T., Zesch, W., Chan, W. P., Kenny, T. W., Fearing, R., and Full, R. J., *Nature* **405**, 681–685 (2000).
- [3] Kendall, K., *Proc. R. Soc. A* **341**, 409–428 (1975).
- [4] Geim, A. K., Dubonos, S. V., Grigorieva, I. V., Novoselov, K. S., Zhukov, A. A., and Shapoval, S. Y., *Nat. Mater.* **2**, 461–463 (2003).
- [5] Hui, C. Y., Glassmaker, N. J., Tang, T., and Jagota, A., *J. R. Soc. Interface* **1**, 35–48 (2004).
- [6] Glassmaker, N. J., Jagota, A., Hui, C.-Y., and Kim, J., *J. R. Soc. Interface* **1**, 23–33 (2004).
- [7] Glassmaker, N. J., Jagota, A., and Hui, C. Y., *Acta Biomaterialia* **1**, 367–375 (2005).
- [8] Crosby, A. J., Hageman, M., and Duncan, A., *Langmuir* **21**, 11738–11743 (2005).
- [9] Thomas, T. and Crosby, A. J., *J. Adhes.* **82**, 311–329 (2006).
- [10] Kaelble, D. H., *Trans. Soc. Rheol.* **4**, 45–73 (1960).
- [11] Falconnet, D., Csucs, G., Grandin, H. M., and Textor, M., *Biomaterials* **27**, 3044–3063 (2006).
- [12] Mitchell, S. A., Poulsson, A. H. C., Davidson, M. R., Emmison, N., Shard, A. G., and Bradley, R. H., *Biomaterials* **25**, 4079–4086 (2004).
- [13] Pallandre, A., Glinel, K., Jonas, A. M., and Nysten, B., *Nanoletters* **4**, 365–371 (2003).
- [14] Wier, K. A., Gao, L., and McCarthy, T. J., *Langmuir* **22**, 4914–4916 (2006).
- [15] Ahagon, A. and Gent, A. N., *J. Polym. Sci.* **13**, 1285–1300 (1975).
- [16] Ramrus, D. A. and Berg, J. C., *J. Adhesion Sci. Technol.* **18**, 1395–1414 (2004).
- [17] Cook, J. and Gordon, J. E., *Proc. R. Soc. A*, 508–520 (1964).
- [18] Chung, J. Y. and Chaudhury, M. K., *J. R. Soc. Interface* **2**, 55–61 (2005).
- [19] Varenberg, M., Peressadko, A., Gorb, S., and Arzt, E., *Appl. Phys. Lett.* **89**, 121905 (2006).